Direct measurement of the evanescent field profile produced by objective-based total internal reflection fluorescence

Alexa L. Mattheyses
University of Michigan
Biophysics Research Division
Ann Arbor, Michigan 48109
E-mail: amatthey@umich.edu

Daniel Axelrod
University of Michigan
Biophysics Research Division
and
Department of Physics
Ann Arbor, Michigan 48109

Abstract. Total internal reflection fluorescence (TIRF) microscopy produces a thin excitation field (the evanescent field) that nominally decays exponentially. This field is ideal for selective excitation of fluorophores near the coverslip/sample interface. We present an experimental method, where the depth and axial profile of the evanescent field can be measured directly by microscopic observation of low refractive index fluorescently labeled spherical beads in an index-matched solution. To demonstrate the technique, through-the-objective TIRF is set up with laser excitation. In this configuration, the axial profile of the evanescent field created by either a 1.45-numerical aperture (NA) or a 1.65-NA objective fits well to a double exponential. At the coverslip/sample interface, about 90% of the evanescent field is represented by an exponential with a decay rate consistent with that expected for a theoretical evanescent field; the remaining 10% of the field is represented by an exponential with a much longer decay constant and is identified as scattering. The approach presented here is particularly useful for investigating the quality and axial profile of the evanescent field in both laser-based and mercury arc-based through-the-objective TIRF systems where a significant amount of light scattering can occur in the illumination optics. [DOI: 10.1117/1.2161018]

Keywords: total internal reflection fluorescence; evanescent field profile; microscopy; index matching.

Paper 05022R received Jan. 28, 2005; revised manuscript received Aug. 8, 2005; accepted for publication Aug. 29, 2005; published online Jan. 24, 2006.

1 Introduction

The study of biochemical and biological processes and of single molecules at a liquid/solid interface has been greatly aided by total internal reflection fluorescence (TIRF) microscopy.[1] TIRF creates an evanescent excitation field intensity that decreases with distance into the liquid. Because of this unique intensity profile, only fluorophores at or very near the liquid/solid interface (within 100 to 200 nm) are excited, and virtually all fluorescence from molecules in the bulk liquid is eliminated. Another benefit of TIRF is that the exponential decay of the evanescent field can be used to make quantitative calculations of movements perpendicular to the surface. This has been exploited to measure the displacement of secretory granules to and from the cell/substrate interface.[2]

An evanescent field is produced when an excitation light beam traveling in a solid (such as a glass coverslip) is incident on an interface with a liquid at an angle θ greater than the critical angle (measured from the normal). The critical angle θ_c is a function of the indices of refraction of both the glass coverslip (n_3) and the liquid (n_1):

$$\theta_c = \sin^{-1}(n_1/n_3). \tag{1}$$

Theoretically, the axial profile of the evanescent field can be precisely calculated. It is an exponentially decaying field in the direction normal to the surface (the z axis), the depth d of which is given by:

$$d = \frac{\lambda_o}{4\pi n_3}(\sin^2\theta - \sin^2\theta_c)^{-1/2}, \tag{2}$$

where λ_o is the vacuum wavelength of the incident light, and θ is the angle from the normal at which the light is incident on the surface.

The optical configurations typically employed in TIRF microscopy fall into two categories, prism (or condenser)-based and through-the-objective.[1] When TIRF is set up in the through-the-objective configuration for biological imaging, several practical considerations make the calculation of d an approximation at best. First, it is difficult to accurately determine all the parameters involved, particularly the angle of incidence of the light and the (possibly heterogeneous) refractive index n_3 of the biological sample. The second uncertainty, addressed by this work, is that it is not known if the

Address all correspondence to Alexa L. Mattheyses, University of Michigan, Biophysics Research Division, 930 N. University, Ann Arbor, Michigan 48109. Tel.: 734–764–5280; Fax: 734–764–3323; E-mail: amatthey@umich.edu

1083-3668/2006/11(1)/014006/7/$22.00 © 2006 SPIE

actual field created by through-the-objective TIRF is purely exponential in practice. The excitation beam could scatter while passing though the objective, thereby causing some light to be incident on the sample/coverslip interface at angles other than θ_c, including some subcritical angles. The result would be a mixture of propagating light with the evanescent field. Indeed, such errant scattering can be observed by eye in a sample consisting of an aqueous fluorescent solution under TIRF illumination. One obvious type of scattering leads to bright, collimated shafts of light emanating from the periphery of the objective's top lens. Fortunately, these collimated rays do not traverse the field of view. However, also visible in the fluorescent solution is a dim diffuse isotropic scattering that does enter the field of view. The goal of this work is to determine the relative contribution of the nonevanescent illumination impurity in the observation volume, its contribution to the excitation field, and how it depends on incidence angle and microscope objective.

The intensity of the evanescent field may be sensed by a fluorescent probe. A challenge in measuring the evanescent field is to avoid disrupting it. One nondisruptive method for measuring evanescent field depth has been reported by Harlepp et al.[3] Their method uses a sample of free fluorophores along with fluorescence correlation spectroscopy (FCS) to determine the field depth. This FCS method measures very precisely the penetration depth of the field, assuming a single exponential, but cannot describe its z profile. Another technique does define the z profile and utilizes a fluorescent probe, either a bead or a quantum dot, on the tip of an atomic force microscope (AFM) cantilever tip.[4] With the AFM method, a strictly exponentially decaying field in z with no scattering was reported. Although this result nicely matches the expectations of simple TIRF theory, it is also surprising because (as mentioned before) a scattering contribution can be seen qualitatively by the eye in fluorescent solutions (although possible background subtraction may have obscured quantitative evidence of scattering). The AFM result is also perhaps surprising because, regardless of the z profile of excitation, the efficiency of light collection emitted from an excited fluorophore should be a function of z due to fluorophore near-field interactions and far-field reflections at the surface (the relevant theory for classical emission dipoles has been well studied, although it may be different for quantum dots; see the discussion in Sec. 4). This collection efficiency effect should distort the fluorescence profile away from a pure exponential.

To determine the z profile directly, it is desirable to use a single probe large or bright enough to track. However, if such a probe has different refractive index than the surrounding liquid, the material will scatter light. A spherical probe unmatched in refractive index converts evanescent light into propagating beacons outside the sphere. This can be seen readily in fluorescent solution [Fig. 1(a)]. (The intensity pattern inside a sphere can be even more complicated.[5]) However, if the index of refraction of the surrounding media and the probe object are equal, there will be no dielectric boundary and the evanescent field will remain pure and unscattered. Index matching places a significant restriction on the types of materials appropriate for the probe object. The index of refraction of the sample must be lower than that of the glass coverslip to satisfy the physical requirements for total internal reflection.

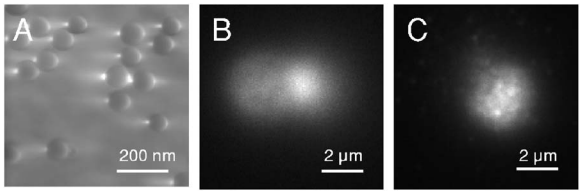

Fig. 1 Index-matching effect. Matching the index of refraction of the bead with the solution eliminates perturbation of the evanescent field by the bead. (a) High index of refraction unlabeled beads (n=1.51) in fluorescent solution at n_1=1.33. Note the comet-shaped beacons of propagating light that the beads have generated from evanescent light. The focus is at the equatorial plane of the beads. (b) A lower index bead (n=1.42) diI-coated on its surface, in unlabeled aqueous (n=1.33) solution, still not index matched. The double "ghost image" of the bead is caused by nonuniform illumination inside the bead as it converts some of the evanescent field into propagating light. (c) The same type of fluorescently coated bead as in (b), except here in an index-matched glycerol/water solution. Only one image of the bead is seen and there are no apparent effects of perturbation of the evanescent field. In both (b) and (c), the microscope is focused on the coverslip surface, and the visible "splotch" of fluorescence is only that portion of the bead in close contact with the coverslip; the full bead is much larger.

The method presented here for experimentally probing the z profile and purity of the evanescent field uses a large diameter sphere made of a low index of refraction material (n=1.42), fluorescently labeled on its surface, and bathed in an index-matched media [see Fig. 1(c)]. Based on the geometry of the sphere, this sample offers an approach for quantifying the fluorescence response as a function of z distance from the surface. This method requires no special equipment and allows full investigation of the depth and purity of the evanescent field, and is demonstrated here with through-the-objective TIRF.

2 Materials and Methods

2.1 *Sample Preparation*

Silica microspheres (8.85 μm diameter) were purchased from Bangs Laboratories (Fishers, Indiana). The beads were prepared on the day of the experiment by coating them with 3,3′ dioctadecylindocarbocyanine (diI-C_{18}-3, diI, Molecular Probes, Incorporated, Eugene, Oregon) by immersion in a saturated diI-ethanol solution, followed by multiple rinses with water. Immediately before observation, the beads were suspended in an index-matched glycerol/water solution and allowed to settle on the surface of a coverslip. The beads are not chemically attached to the surface and are held there only weakly by gravity; their large size minimizes any significant Brownian motion. Under these circumstances, distortion of the bead's spherical shape should be minimal.

The solution index matched to the beads was found by scattering minimization of the beads in a series of glycerol-water mixtures under dark-field microscopy. The refractive index of the beads is advertised as 1.37; however, their scattering minimum was in a 70% glycerol/water (v/v) solution, which has an index of refraction of 1.42, as published in physical tables and confirmed with an Abbe refractometer.

2.2 *Optical Setup and Image Acquisition*

Through-the-objective TIRF was set up on an Olympus IX70 microscope. A 488-nm wavelength laser beam from an argon laser (a 100-mW total power model is easily sufficient) was directed through a custom-fabricated side port and focused on the back focal plane of the objective. The radial position of the focused beam on the back focal plane (and therefore the incidence angle) was manually adjustable. The filter cube contained a 495 long-pass dichroic mirror and 500-nm long-pass emission filter (Chroma Technology Corporation, Rockingham, Vermont). The objectives used were an Olympus 60 $\times$1.45 NA (n_3=1.515 oil and coverslip) and the Olympus 100$\times$1.65 NA (n_3=1.78 oil and coverslip). All images were acquired while focused at the coverslip/sample interface. Images were recorded with a cooled charge-coupled device (CCD) camera (Sensicam, Cooke Corporation, Romulus, Michigan) with the camera's Sensicontrol software. The exposure times were 400 ms (1.45 NA) and 500 ms (1.65 NA).

2.3 *Supplementary Measurement of Incidence Angle*

To check the accuracy of the decay constant measured with our bead technique, we calculated the theoretical depth d of the evanescent field from Eq. (2), based on an experimentally estimated angle of incidence θ. Angle θ is adjustable by a lens in the beam (mounted on a micrometer translator) that controls the radial position of the laser beam focus at the objective's back focal plane. A triangular (45-45-90) glass prism is placed on the stage and coupled to the objective with emersion oil. At various micrometer settings, even those that would produce TIR at a typical sample interface with an aqueous medium, the laser light propagates into the prism, finally creating a spot on the wall. After some simple measurements and the application of Snell's law, the angle at which the light emerges from the objective can be determined. The incidence angles created at many micrometer settings were measured, and a graph relating micrometer translator position to incidence angle was created. This procedure was performed for the 1.45-NA objective only. The actual spread of angles in the putatively collimated incidence beam can be judged from the width of the spot on the wall; it is less than ±0.5 deg around its central direction.

2.4 *Image Analysis*

Image analysis was performed by programs custom designed in Interactive Data Language (IDL, Research Systems, Incorporated, Boulder, Colorado) by the authors. The aim of the image analysis is to determine the z-dependent intensity profile from images of beads. First, the coordinates of the center of each bead were determined to one-pixel accuracy by convolving the experimental image with a computer-generated image of a solid circular disk. Then, subpixel accuracy was obtained from the peaks of parabolas determined by the intensities of the center pixel and each of the two immediately adjacent pixels in each dimension. This provides a center position with coordinates (X,Y). The background was calculated as the average intensity of pixels in a doughnut 17 pixels wide with an inner radius larger by 10 pixels than the radius of the visibly illuminated bead image. This background value was subtracted from every position in the image. All the pixels inside the image area of the projected sphere were assigned a radial bin based on their position $(x+0.5, y+0.5)$ [where (x,y) is the position of the lower left corner of a pixel] and their distance from the center of the bead (X,Y). These radial bins recorded the average intensity I' of all pixels that fall within the same one-pixel-wide range of radius r from the bead center. The azimuthal angle averaging was necessary, because the bead surface showed small irregularities due to uneven labeling. Then each r was converted into a z distance using the known geometry of the sphere, where the radius of the bead is R=4.445 μm (see Fig. 2):

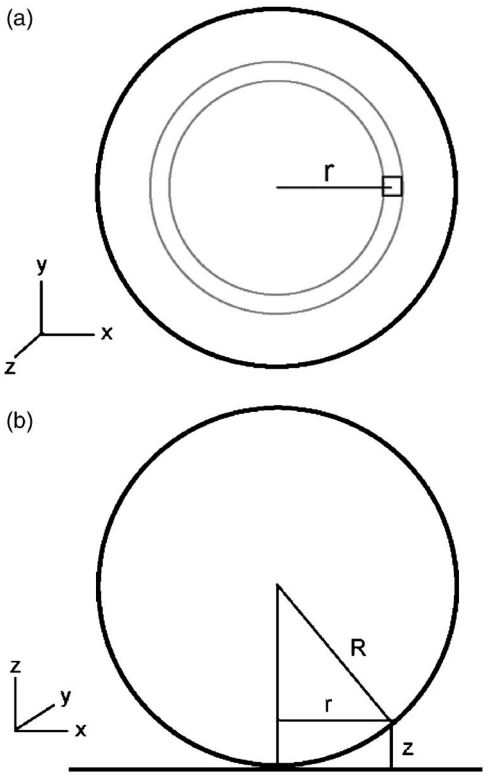

Fig. 2 Schematic drawing of optical geometry. (a) View of bead in x-y plane as observed though the microscope. The ring outlined in gray is one radial bin wide, corresponding to radius x. One square pixel in that ring is shown. (b) View of the cross section of a bead resting on a coverslip in x-z plane, showing the conversion of projected x radius into a z distance from the coverslip.

$$R^2 = r^2 + (r - z)^2. \tag{3}$$

This analysis results in the fluorescence intensity I' as a function of z. Next, I' was adjusted to correct for the difference in the surface area of the bead projected into every pixel to give the normalized intensity I for each z:

$$I = I' \cos[\sin^{-1}(x/R)]. \tag{4}$$

The result was clearly not a single exponential. To better represent the I versus z profile, it was fit to a double exponential:

$$I = A \exp(-Bz) + C \exp(Dz). \tag{5}$$

This procedure was repeated for ten beads at each field depth. Of the ten, any with an average deviation of the fit

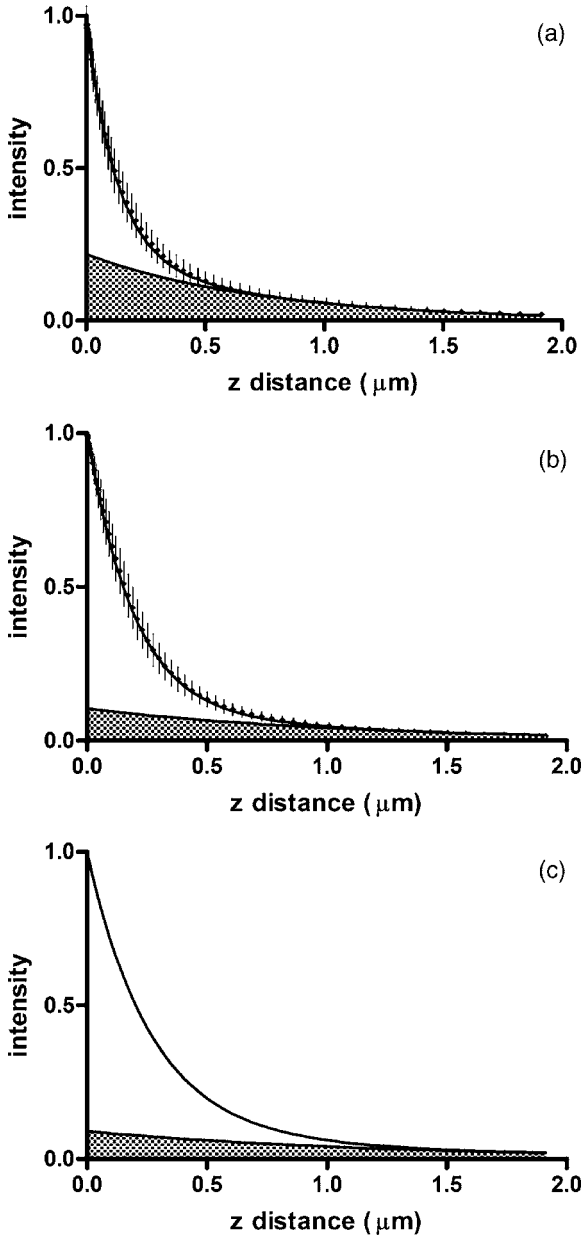

Fig. 3 Intensity versus z for the 1.45-NA objective lens. Experimental data (diamonds with standard deviation error bars centered on the mean, as averaged over all useable beads) as well as complete fit curve. The slow-decaying scatter portion of the fit curve is also plotted (gray filled). The depths from the fast decay are (a) 125 nm, (b) 188 nm, and (c) 264 nm.

curve from the data points (averaged over all the data points) of greater than 0.05 (with curves normalized to unity at $z=0$) were discarded. This criterion was designed to discriminate against images with anomalous bits of fluorescent debris and never more than three of the beads from a given experiment, and often none of the beads were discarded. The curves of all the remaining beads were averaged to create the experimental curve, and their fit parameters were averaged to create the average fit. The excitation field appeared homogeneous over most of the lateral (x-y) field-of-view plane, and the beads were always imaged at the same location in the field.

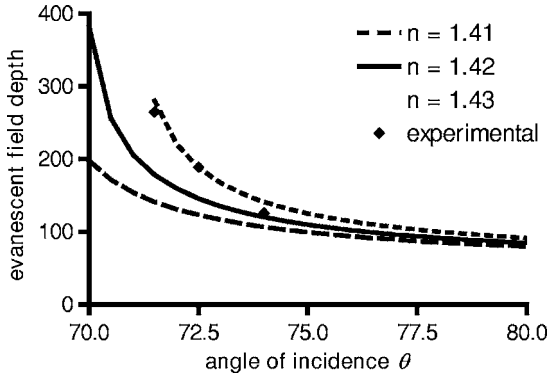

Fig. 4 Evanescent field depth versus measured angle of incidence. The curves on this plot show theoretically calculated evanescent field depths (defined as the 1/e characteristic exponential distance) where the wavelength=488, the index of refraction of glass=1.515, and the index of refraction of the sample takes on three different values: n_1 =1.43 (dotted); 1.42 (solid); and 1.41 (dashed). These different indices of refraction curves illustrate the sensitivity of the field depth to index of refraction at angles close to the critical angle. The data points (diamonds) represent the three experimental field depths (i.e., the 1/e characteristic distance of the fast-decaying component only) using the bead method here, for the 1.45-NA objective. The angle values on the abscissa were obtained by matching the micrometer readings to the calculated incidence angles. The match of the data points to the theoretical curves at close to the expected refractive index (1.42) confirms the identification of the fast-decaying component of experimental intensity versus z curves with the theoretical evanescent field.

Note that the intensity I refers to the fluorescence intensity, not the excitation field intensity. The two are almost, but not quite, proportional to each other. An additional factor involving the efficiency of fluorescence collection as a function of z must be considered (see the discussion in Sec. 4).

3 Results

Three different evanescent field depths were probed using the 1.45-NA objective. For each incidence angle, ten different beads were individually imaged. The intensity profiles for each incidence angle were determined as described in Sec. 2. The z-dependent axial intensity profiles are shown in Fig. 3. At small z distances, the majority (90%) of the signal corresponds to a fast exponential, the depth of which corresponds to the expected depth of the evanescent field. The rest of the field, 10%, corresponds to a slow exponential. We attribute the existence of this slow exponential component to light scattering in the objective. As the z distance increases, the evanescent contribution decreases, and putative scattered light dominates the excitation field. The percentage of the "scatter" contribution at $z=0$ increases as the incidence angle increases with the 1.45-NA objective.

The corresponding incidence angles for the micrometer readings were determined by the prism method. The evanescent depths (attributed to the fast exponential) are in agreement with those theoretically calculated for n_1 $=1.425\pm0.005$ (Fig. 4). The derived n_1 of 1.425 is close to the actual n_1 of 1.42, which strengthens the interpretation that the fast component of the bead intensity versus z decay corresponds to the TIR evanescent field.

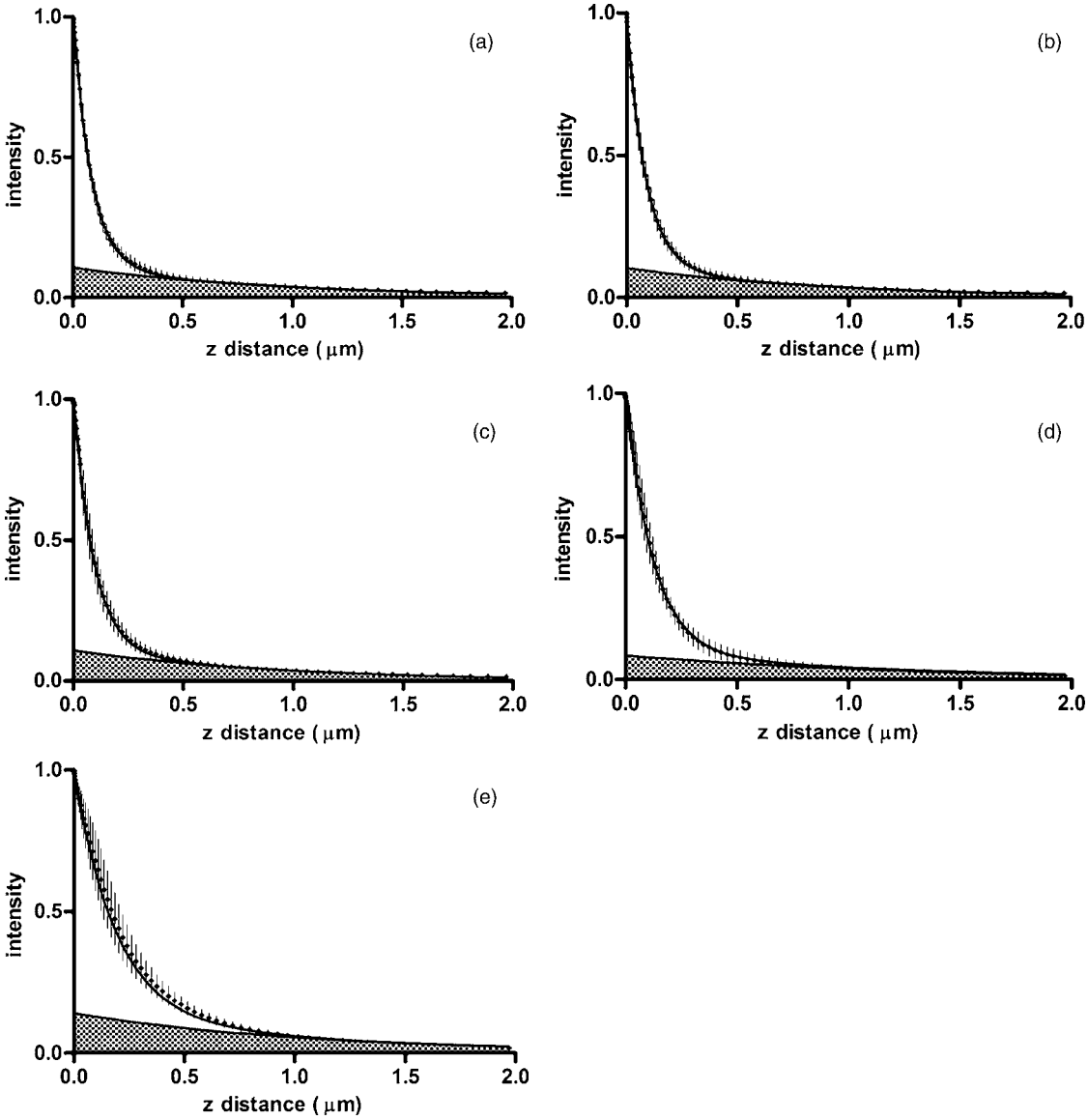

Fig. 5 Intensity versus z for the 1.65-NA objective lens. Experimental data (diamonds with standard deviation error bars centered on the mean, as averaged over all useable beads) as well as complete fit curve. The slow-decaying scatter portion of the fit curve is also plotted (gray filled). The depths from the fast decay are (a) 83 nm, (b) 85 nm, (c) 91 nm, (d) 121 nm, and (e) 185 nm.

Five incidence angles were investigated with the 1.65-NA objective. The intensity profiles for each incidence angle were found as described in Sec. 2. The average fits to a double exponential are shown in Fig. 5. Similar to the 1.45-NA objective, 90% of the excitation intensity at $z=0$ is from the evanescent field, and 10% is from scatter. Unlike the 1.45-NA objective, with the 1.65-NA objective, the percentage of scatter remains steady at 10% for all incidence angles investigated.

4 Discussion

We present a simple method for experimentally measuring the axial profile of the evanescent field produced by TIR. The method involves observation of fluorescently labeled low index of refraction microspheres in an index-matched solution, followed by a simple image analysis protocol. The axial (z) field profile fits well to a double exponential, the rapid decay term of which is in reasonable agreement with the expected evanescent field depth (for the 1.45-NA objective), and the other of which has a much longer decay and is attributed to scattering in the objective. The shortest evanescent decay depth measured here for the 1.45-NA objective is 125 nm.

Estimations of incidence angle and evanescent field depth are not available directly for the 1.65-NA objective for this series of experiments. However, in an experimental series by Allersma et al.,[2] the evanescent field depth produced by the 1.65-NA objective is around 55 nm, as estimated by the prism method described earlier. The depth inferred from the short decay component here is somewhat longer, in the 85-nm range. However, most of that difference is accounted for by different refractive indices of the respective liquids; the index assumed by Allersma et al. was 1.38, whereas the index was

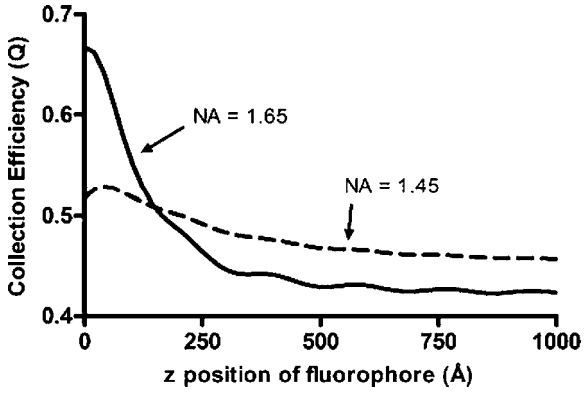

Fig. 6 Theoretical calculation [based on numerical integration of Eqs. (;46) through (49) in Hellen and Axelrod[8]] of the collection efficiency (Q) of objectives with numerical aperture 1.45 (dashed line) and 1.65 (solid line) from a randomly oriented excited fluorophore as a function of z distances. Note that the 1.65-NA objective uses high-index oil and coverslips (n_3=1.78), whereas the 1.45 objective uses standard oil and coverslips (n_3=1.52). The substrate refractive index affects the emission pattern, and that effect is implicitly included here. Note that the 1.65 NA is more efficient than the 1.45 NA for collecting proximal fluorophore emission, but less efficient for distal fluorophores emission; once a fluorophore is too far to couple its near-field into the glass, both objectives gather all of the light that refracts into the glass. But the lower n_3 used with the 1.45 NA supports less reflection into the liquid and thereby more refraction into the glass and objective.

1.42 here. In addition, Allersma et al. used different (possibly larger) radial positions for the focused laser focal at the back focal plane. In either case, the decay depths accessible by the 1.65 objective are clearly significantly shorter than those for the 1.45-NA objective, as is expected.

The exponential term corresponding to evanescent field depth is approximately 90% of the total field intensity at z =0. At small z distances, the field is dominated by the fast exponential term, but at large z, the slow-decaying scattering becomes the dominant factor. If one uses the oversimplified assumption of a single exponential excitation field, this scattering will lead to a computed underestimate of the actual distance at which more distant fluorescent objects reside. For example, an object that is in reality located at z=170 nm [twice the fast evanescent field component depth d=85 nm, depicted in Fig. 5(b)] will report an intensity (relative to the z=0 value) larger than expected for an object at that distance from a single exponential of d=85 nm, corresponding to a calculated position of only 131 nm.

The slow-decaying scattering component probably originates within the objective. There are two distinct types of scatter that exist. Bright shafts of laser light are visible in a fluorescent solution with both of the objectives in TIR mode, emanating off-axis from the edges of the top lens. Fortunately these bright, collimated shafts do not traverse the field of view. A second dimmer and more diffuse type of scattered light is also observed. This contribution probably accounts for the slow-decaying field we observe. Our representation of the scattering component by a long decaying exponential is only a mathematical convenience; there is no reason to think that it is really an exponential at all. It is probably closer to a function with an even longer tail (such as an inverse power function $z^{-\beta}$).

The source of the scattered light is most likely multiple reflections at various surfaces and scattering in elements in the objective. The amount of scatter remained constant for different incidence angles as well as for the different objectives. Only for the largest incidence angle with the 1.45-NA objective was there an increase in scatter observed. This is most likely because the laser beam was traveling very close to the edge of the objective at this angle and grazed the limiting aperture. Nonetheless, for most angles used, the scatter does not depend on the incidence angle, so grazing the edge does not seem to be a problem except at the largest radial positions in the back focal plane.

The measurement-based calculations of the rapidly decaying exponential component here agree well with the predictions based on the actual incidence angle. This agreement means that the prism-based method can be used reliably to predict incidence angle, and thereby to calculate the depth of the evanescent field. The prism-based method and calculation still involves an estimation of the index of refraction of the sample. The benefit of the bead technique presented here is that it provides an exact intensity profile and thereby reveals information on the amount of scattered light.

This technique demonstrates the degree of purity of objective-based, through-the-lens TIRF illumination. The refractive index used here (1.42) is not far from above the average refractive index of most cells (1.38 to 1.42). But in a cell, the local refractive index is both poorly known and heterogeneous. These features will affect both the actual evanescent depth and possibly introduce more scattering, as seen by fluorophores on the sample.

Technically, it is not the intensity of the excitation evanescent field (plus scattering) that is being measured and plotted by this technique. Rather, it is the product of two terms: the intensity of excitation and the efficiency of emission collection, and both terms are functions of fluorophore z distance from the surface.[6–8] A program was written to calculate the collection efficiency of different objectives (with the corresponding recommended refractive indices of the coverslip and immersion oil), based on Eqs. (46) through (49) presented in Hellen and Axelrod.[8] Typical results are shown in Fig. 6, where collection efficiency Q is the fraction of emitted light that is actually captured by the objective (viewing through a glass coverslip) from an excited fluorophore at axial position z. Clearly, the effect is significant: well over 50% of the emitted light is captured for proximal fluorophores, because the interaction of the fluorophore's near-field with the glass surface produces a bias toward emission into the substrate and subsequently into the objective. Conversely, for more distal fluorophores, collection through the glass coverslip suffers because some of the far-field emitted light reflects off the glass back into the liquid. This surface-selective effect for collection efficiency is the strongest for the 1.65-NA objective. The result will always be an *apparent* "evanescent field depth" that is shorter than the actual depth, and a clear deviation from pure exponentiality. It is important, therefore, to measure the *apparent* field depth through the same optics (objective and substrate) that will be used in actual experiments, as can be done here with the bead technique. Note that this collection

efficiency effect does *not* account for the long-decaying component seen experimentally here; its main effect is to increase the steepness of the decay from pure single exponentiality.

The bead method presented here will be useful for evaluating the purity of the evanescent field created in many different experimental setups with varying alignment, objective type, excitation wavelength, and manufacturer, including the new Hg-arc-based TIRF commercial systems, where impurities due to propagating light are likely.

Acknowledgments

We thank Miriam Allersma for the prism-based measurement of incidence angles. This work was supported by NIH R01-NS38129 to Axelrod and a NIH Molecular Biophysics Training Grant Fellowship and a Guidant Award Fellowship to Mattheyses.

References

1. D. Axelrod, "Total internal reflection fluorescence microscopy in cell biology," *Methods in Enzymology*, pp. 1–33, Academic Press, San Diego (2003).
2. M. W. Allersma, L. Wang, D. Axelrod, and R. W. Holz, "Visualization of regulated exocytosis with a granule membrane probe using total internal reflection microscopy," *Mol. Biol. Cell* **15**(10), 4658–4668 (2004).
3. S. Harlepp, J. Robert, N. C. Darnton, and D. Chatenay, "Subnanometric measurements of evanescent wave penetration depth using total internal reflection microscopy combined with fluorescence correlation spectroscopy," *Appl. Phys. Lett.* **85**(17), 3917–3919 (2004).
4. A. Sarkar, R. B. Robertson, and J. M. Fernandez, "Simultaneous atomic force microscope and fluorescence measurements of protein unfolding using a calibrated evanescent wave," *Proc. Natl. Acad. Sci. U.S.A.* **101**(35), 12882–12886 (2004).
5. C. Liu, T. Kaiser, S. Lange, and G. Schweiger, "Structural resonances in a dielectric sphere illuminated by an evanescent wave," *Opt. Commun.* **117**, 521–531 (1995).
6. J. Enderlein, T. Ruckstuhl, and S. Seeger, "Highly efficient optical detection of surface-generated fluorescence," *Appl. Opt.* **38**(4), 724–732 (1999).
7. W. Lukosz and R. E. Kunz, "Light emission by magnetic and electric dipoles close to a plane interface. I. Total radiated power," *J. Opt. Soc. Am.* **67**(12), 1607–1614 (1977).
8. E. H. Hellen and D. Axelrod, "Fluorescence emission at dielectric and metal-film interfaces," *J. Opt. Soc. Am. B* **4**(3), 337–350 (1987).